Electronic Supplementary Material (ESI) for Physical Chemistry Chemical Physics.
This journal is © the Owner Societies 2016

Supporting information for: Multiscale computational modeling of ^{13}C DNP in liquids

Sami Emre Küçük and Deniz Sezer*

Faculty of Engineering and Natural Sciences, Sabancı University, Orhanlı-Tuzla, 34956 Istanbul, Turkey

E-mail: dsezer@sabanciuniv.edu

MD simulations

Acetone in water

Molecular dynamics (MD) simulations of 1 TEMPOL, 1029 acetone and 7433 water molecules in a cubic box were carried out with NAMD.[S1] The parameters of acetone and (TIP3P) water were from the CHARMM36 molecular force filed.[S2] Parameters of TEMPOL have been developed previously.[S3] Temperature of 25 °C and pressure of 1 atm were maintained with Langevin thermostat and barostat. The average box size was 6.98 nm, leading to acetone concentration of 5 M, in agreement with experiment.[S4] In order to reproduce the experimental translational diffusion constant of acetone in water reported to be $D = 1.10$ nm^2/ns,[S4] the friction coefficient of the Langevin thermostat was chosen as 4.35 ps^{-1}.[S5] The resulting coefficients of translational diffusion of acetone and TEMPOL are given in Table S1. MD simulations were carried out for 10 ns and coordinates were recorded every 0.2 ps, yielding 50 thousand snapshots for analysis.

In addition to the translational diffusion of the molecules in the liquid, their rotational diffusion is also expected to influence the frequency-dependence of the dipolar interaction between the electron and nuclear spins. Therefore, the time scales of rotation should also be assessed. We have previously reported such an assessment for pure acetone.[S5]

Table S1: Diffusion coefficients (nm^2/ns) as obtained from the MD simulations.

	D_{solvent}	D_{TEMPOL}
5 M acetone (in water)	1.10 ± 0.01	0.43 ± 0.13
chloroform	2.86 ± 0.44	2.62 ± 1.19

Chloroform

MD simulations of 1 TEMPOL and 2741 chloroform molecules, with chloroform parameters obtained from the literature,[S6] were performed at 25 °C and 1 atm, yielding an average box size of 7.17 nm. A thermostat friction of 0.014 ps^{-1} was employed to match the experimental diffusion coefficient of chloroform ($D = 2.8$ nm^2 ns^{-1}).[S7] The resulting diffusion coefficients of chloroform and TEMPOL are given in Table S1. The MD simulations were carried out for a total duration of 10 ns. Snapshots were saved every 0.1 ps, yielding 100 thousand frames for analysis.

The fidelity of the orientational motion of the simulated chloroform molecules was assessed through an analysis of the complex frequency-dependent dielectric response.[S5] To this end, the time correlation function (TCF) for the electric dipole moment of the simulated system is calculated as follows:

$$\Phi(t) = \Big\langle \mathbf{M}(\tau)\mathbf{M}(t+\tau) \Big\rangle_{\tau}. \tag{1}$$

Here $\mathbf{M}(t)$ is the total dipole moment vector of the simulation box at time t, and pointed brackets indicate averaging over the time τ. Assuming rotationally isotropic motion, cross terms between Cartesian coordinates are zero and another average can be taken over the three Cartesian coordinates.

The frequency-dependent dielectric function can be written as

$$\epsilon(\omega) = \epsilon(\infty) - \frac{1}{Vk_{\mathrm{B}}T\epsilon_0}\int_0^\infty \dot{\Phi}(t)\mathrm{e}^{-\mathrm{i}\omega t}\mathrm{d}t, \tag{2}$$

where V is the volume of the simulation box, k_{B} is Boltzmann's constant, T is temperature, ϵ_0 is the permittivity of free space, and the dot above Φ indicates a derivative with respect to time. We fit the TCF obtained from the MD simulations to a sum of decaying exponential functions:

$$\Phi(t) = \sum_i a_i \mathrm{e}^{-t/\tau_i}. \tag{3}$$

With the magnitudes a_i having dimension of Debye squared, a good fit to the TCF of chloroform was obtained with two exponentials: $a_1 = 3346.5$, $\tau_1 = 5.223$ ps and $a_2 = 447.83$, $\tau_2 = 15.32$ ps. Then the real (ϵ') and imaginary (ϵ'') parts of the dielectric function become:

$$\epsilon(\omega) = \epsilon' + \mathrm{i}\epsilon'' = \left[\epsilon(\infty) + \sum_i \frac{a_i}{1+(\tau_i\omega)^2}\right] + \mathrm{i}\left[\omega\sum_i \frac{a_i\tau_i}{1+(\tau_i\omega)^2}\right]. \tag{4}$$

In Fig. S1 we compare the calculated real and complex parts of the dielectric response function with experiment.[S8]

Although in our previous analysis of pure acetone we had $\epsilon(\infty) = 1$,[S5] the experimental data of chloroform (black symbols) shows that $\epsilon(\infty) = 2.26$. To plot the dielectric response according to the MD simulations (solid green lines), the experimental value of $\epsilon(\infty)$ was used together with the a_i and τ_i values obtained from the fit to the TCF. Clearly, the magnitude of the calculated complex response function is larger than the experiment. Indeed, while the experimental dielectric constant is $\epsilon(0) = 4.72$,[S8] the MD-deduced value, obtained after adding $\epsilon(\infty) = 2.26$, is $\epsilon(0) = 5.30$.

Although the dielectric properties of the simulated chloroform liquid are important, our main goal is to assess the *time scales* of the rotational motion of the solvent molecules. In order to directly compare the times scales of the dielectric response, we rescale the magnitude

of the MD-estimated $\epsilon(\omega)$ such that it produces the correct zero-frequency value $\epsilon(0) = 4.72$. The imaginary and real parts of the rescaled function are shown in Fig. S1 with dashed green lines. They are seen to be in almost perfect agreement with experiment, demonstrating that the frequencies of rotation of the simulated chloroform molecules are quantitatively realistic, in spite of the fact that the magnitude of the electric dipole moment is somewhat larger than what it should be.

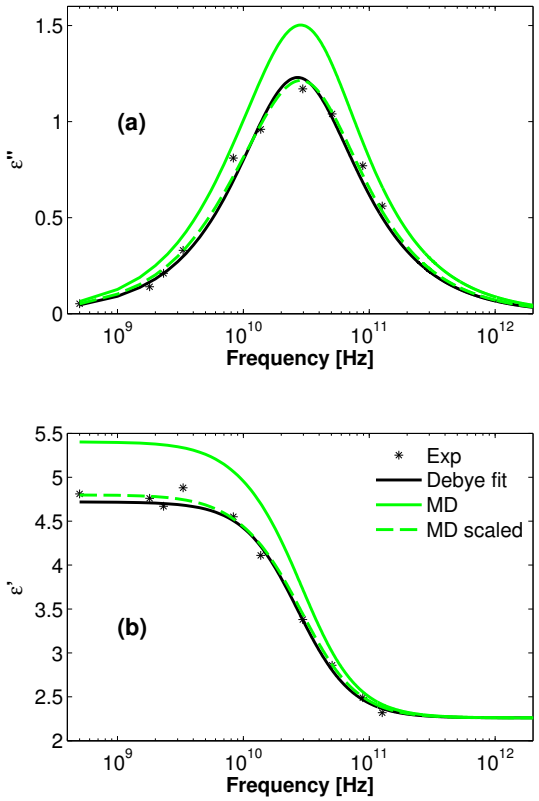

Figure S1: (a) Imaginary and (b) real part of the dielectric response function for chloroform. Experimental data are shown with black symbols. Debye fit to the experimental data, yielding $\epsilon(\infty) = 2.26$, is shown with black solid line. Green solid lines correspond to the functions in square brackets in (4) plotted using a_i and τ_i deduced from fit to MD and $\epsilon(\infty)$ from experiment. The dashed green lines are the MD estimate of $\epsilon(\omega)$, after rescaling such that it matches the experimental zero-frequency value $\epsilon(0) = 4.72$.

DFT calculations

Acetone in water

All DFT calculations were performed using the package Gaussian 09.[S9] For each MD snapshot the coordinates of the 2 acetone and 15 water molecules that were closest to the TEMPOL oxygen atom were retained in the DFT calculation. (The identity of these molecules could change from one snapshot to the next.) The geometries of these molecules were used as as, without optimizing the molecular structures or their relative positions. A continuum polarization model (PCM[S10]) with $\epsilon = 62.5$, corresponding to a 1:3 acetone-water mixture, was employed to account for the dielectric properties of the solution.

Fermi contacts were obtained with the EPR-II basis set[S11] using either B3LYP or BLYP as density functionals. 5000 consecutive MD snapshots, amounting to a total duration of 1 ns, were analyzed with B3LYP. Twice as much (10000) consecutive snapshots, corresponding to 2 ns of molecular dynamics, were analyzed with the BLYP functional. All the calculated Fermi contacts are shown against the distance between the ^{13}C nucleus and the oxygen of TEMPOL in Fig. S2. Here, the Fermi contacts of the carbonyl carbon (a) are above the values of the methyl carbon (b). Somewhat larger Fermi contacts are obtained with BLYP (right) instead of B3LYP (left).

In the case of BLYP, DNP coupling factors were also obtained using only the first 5000 or only the second 5000 snapshots in order to asses the statistical uncertainty in the estimates due to the finite number of calculated Fermi contacts. (The results are shown in Table S5.)

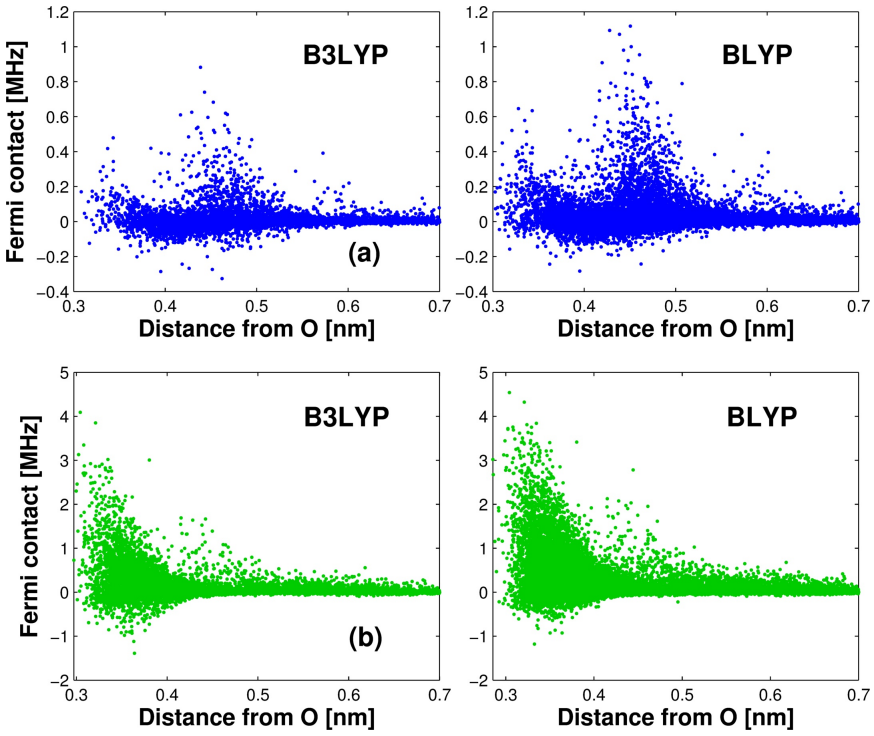

Figure S2: Calculated Fermi contacts for (a) the carbonyl and (b) the methyl carbons of acetone in water. The commonly assumed exponential decay with the distance of the nuclear spin from the electron spin is not observed. Smaller Fermi contacts are obtained with B3LYP (left) compared to BLYP (right).

Chloroform

Because EPR-II is not applicable to chlorine, TZVP[S12] was employed as basis set. Fermi contacts were calculated for one MD snapshot by retaining an increasing number of chloroform molecules (from 1 to 15), in addition to TEMPOL, in the DFT calculation. The calculated Fermi contacts with the carbon on the closest chloroform demonstrate that the numerical values converge quickly with as little as 2 chloroforms present explicitly in the DFT calculation (Fig. S3). Nevertheless, for each MD snapshot we performed a DFT calculation with the 10 chloroform molecules closest to the TEMPOL oxygen explicitly present.

The continuum polarization model SMD[S13] with $\epsilon = 4.7$ was employed to account for the dielectric effect of the rest of the chloroform molecules in the solution. The SMD model was observed to yield slightly larger Fermi contacts in comparison with the PCM model that was employed for the acetone-water mixture above (Fig. S3). However, the difference is much

smaller compared to the difference between B3LYP and BLYP.

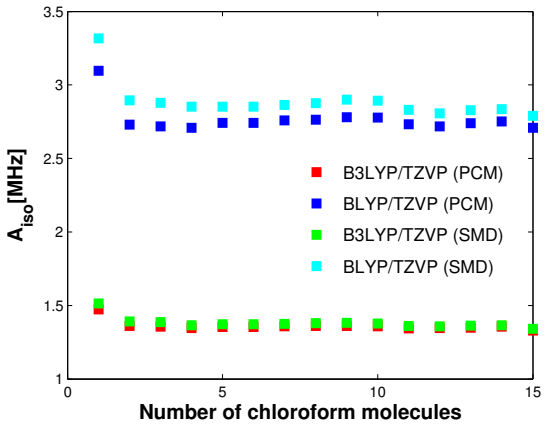

Figure S3: Fermi contact of carbon at the nearest chloroform calculated with increasing number of chloroform molecules around TEMPOL explicitly present in the DFT calculation. The level of theory is either B3LYP/TZVP or BLYP/TZVP, as indicated. The dielectric properties of the environment are accounted for with the continuum dielectric models PCM or SMD.

Fermi contacts from 5000 consecutive MD snapshots (total duration of 0.5 ns) were calculated with B3LYP/TZVP. Again, twice as much (10000) consecutive snapshots were analyzed with BLYP/TZVP. All the calculated Fermi contacts are shown in Fig. S4. In this case, BLYP produces significantly larger Fermi contacts than B3LYP. The magnitudes of the Fermi contacts vary in a complex manner with the distance of the nucleus from the oxygen atom of TEMPOL, making it difficult to model the scalar interaction analytically.

To assess the uncertainty of the estimated DNP coupling factors due to the finite number of DFT calculations, coupling factors were obtained by using only the first half (5000) or the last half (5000) of the Fermi contacts calculated using BLYP. The results are shown in Table S6.

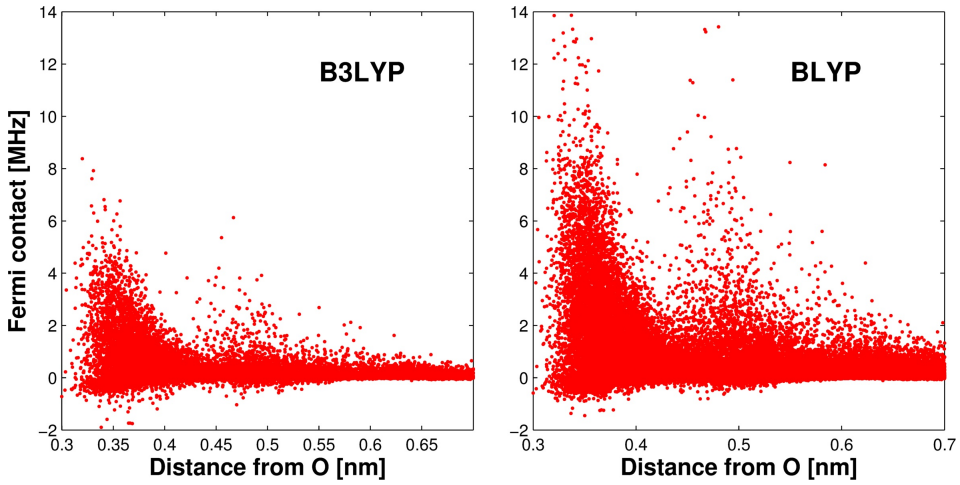

Figure S4: Calculated Fermi contacts as a function of the distance from the chloroform carbon to the TEMPOL oxygen. The functional BLYP (right) produces drastically larger Fermi contacts compared to B3LYP (left).

Calculation of the spectral density functions

Dipolar SDF

The calculation of the spectral density function (SDF) of the dipolar interaction has been described on several occasions before.[S5,S14,S15] In brief, dipolar interactions to nuclei on solvent molecules that are close in space to the free radical are calculated from the positions in the MD simulations. Dipolar interactions to more distant nuclei, all the way to infinity, are accounted for analytically. For this purpose, an imaginary sphere with radius d around the free radical is constructed during the analysis of the MD trajectories (Fig. S5). Defining the inside of the sphere as near region (N) and outside as far region (F), four different time correlation functions (TCFs) are possible according to the region at some time, and time t later. The total dipolar TCF is the sum of these four contributions:

$$C_{\mathrm{dip}}(t) = C^{\mathrm{NN}}(t) + 2C^{\mathrm{NF}}(t) + C^{\mathrm{FF}}(t), \tag{5}$$

where, due to time reversibility, $C^{\mathrm{FN}}(t) = C^{\mathrm{NF}}(t)$ was invoked. Only $C^{\mathrm{NN}}(t)$ and $C^{\mathrm{NF}}(t)$ are obtained from the MD simulations. $C^{\mathrm{FF}}(t)$ is calculated analytically[S14] within the as-

sumptions of the model of diffusing hard spherical molecules with centered spins (HSCS model).[S16,S17]

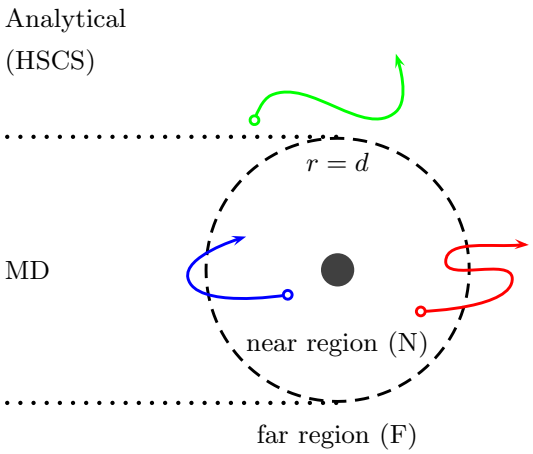

Figure S5: Partitioning of the space around the polarizing agent (dark circle) into near ($r < d$) and far ($r > d$) regions on the basis of the distance r between the free radical and the solvent molecule.[S18] Trajectories of solvent molecules that are in N at two instances separated by time t (blue path) contribute to $C^{\mathrm{NN}}(t)$. Solvent molecules starting in N and moving to F in time t (red path) contribute to $C^{\mathrm{NF}}(t)$. Molecules that are in F at the beginning and end of a time interval of duration t (green path) contribute to $C^{\mathrm{FF}}(t)$. In our analysis $d = 2.5$ nm for both acetone in water and chloroform.

The TCFs $C^{\mathrm{NN}}(t)$ and $C^{\mathrm{NF}}(t)$ are calculated from the recorded MD coordinates as follows:

$$C^m_{\mathrm{dip}}(t) = \frac{2\pi}{5}(\delta_{IS})^2 \langle F^m_{\mathrm{dip}}(\tau) F^m_{\mathrm{dip}}(\tau + t) \rangle_\tau . \tag{6}$$

Here, $F^m_{\mathrm{dip}}(t) = F^m_2(\mathbf{r}(t))$ are the rank-2 solid harmonics, calculated from the spherical polar components of the distance vector between the nuclear and electron spins, $\mathbf{r} = (r, \theta, \phi)$, as

$$F^m_2(\mathbf{r}) = \frac{Y^m_2(\theta, \phi)}{r^3} . \tag{7}$$

The prefactor $\delta_{IS} = (\mu_0/4\pi)\hbar\gamma_I\gamma_S$ in (6) has the value of 1.249×10^{-4} nm^3/ns for ^{13}C. The pointed brackets indicate averaging over the ensemble of molecules and over the time τ. For isotropic liquids the TCFs for $m = 0$, 1 and 2 are all equal, thus the superscript can be dropped. The SDFs corresponding to $C^{\mathrm{NN}}(t)$ and $C^{\mathrm{NF}}(t)$ are obtained by taking the

Fourier-Laplace transform:

$$J^{\mathrm{XX}}_{\mathrm{dip}}(\omega) = \int_0^\infty C^{\mathrm{XX}}_{\mathrm{dip}}(t)\mathrm{e}^{-\mathrm{i}\omega t}\mathrm{d}t, \qquad \mathrm{XX} = \mathrm{NN}, \mathrm{NF}. \tag{8}$$

To perform the Fourier transformation, the near-near (NN) dipolar TCF is first fitted to a sum of exponential decays,

$$C^{\mathrm{NN}}(t) = \sum_i a_i e^{-t/\tau_i}, \tag{9}$$

and subsequently Fourier-transformed as

$$J^{\mathrm{NN}}(\omega) = \sum_i \frac{a_i\tau_i}{1 + (\omega\tau_i)}. \tag{10}$$

The fitting parameters for the methyl (C_{H_3}) and carbonyl (C_O) carbons of acetone, as well as the carbon of chloroform (C) are given in Table S2. The MD estimates and the best multiexponential fits are shown in Fig. S6a.

Table S2: Multi-exponential fit parameters a_i (nm^{-3}) and τ_i (ps) for the dipolar near-near TCFs of carbons of acetone (C_{H_3} and C_O) and chloroform (C). The prefactors $(2\pi/5)$ and $(\delta_{IS})^2$ in (6) are not included in the fits.

	C_{H_3}		C_O		C	
i	a_i	τ_i	a_i	τ_i	a_i	τ_i
1	1.557	0.897	0.737	1.111	0.680	0.731
2	2.537	9.640	2.316	15.18	1.874	6.730
3	2.722	44.76	2.241	52.38	2.771	22.98
4	0.289	204.2	0.218	229.7	0.261	90.31

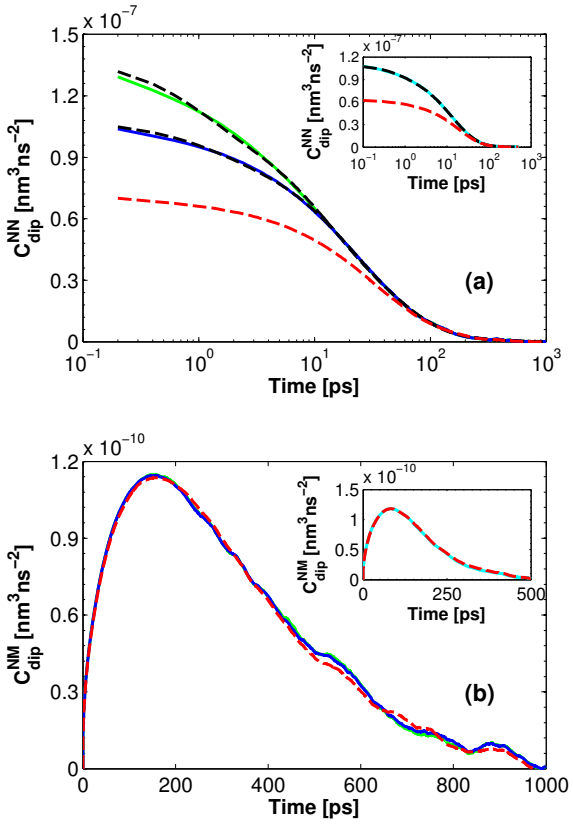

Figure S6: (a) Near-near (NN) and (b) near-intermediate (NM) dipolar TCFs of acetone (main figures) and chloroform (insets). Solid lines show TCFs calculated using the actual positions of C_{H_3} (green), C_O (blue) of acetone, and C of chloroform (cyan). Black dashed lines in (a) show their exponential fits. Red solid lines indicate TCFs calculated by pretending that the nuclear spins are at the centers of mass (COM) of the solvent molecules. The actual spin position becomes immaterial at sufficiently large distances, as demonstrated by $C^{\mathrm{NM}}(t)$ in (b).

Due to the limited size of the MD simulation box, only molecules within a distance less than the simulation box will contribute to the MD estimate of $C^{\mathrm{NF}}(t)$. Formally, however, $C^{\mathrm{NF}}(t)$ should include the contribution of molecular trajectories reaching beyond the MD box, in principle going all the way to infinity. We, therefore, realize that $C^{\mathrm{NF}}(t)$ cannot be estimated directly from MD simulations. To overcome this problem, we introduce another auxiliary sphere centered at the free radical and having a radius $r = a$ (Fig. S7). When calculating TCFs from the MD trajectories we pretend that molecules crossing the surface of this outer sphere disappear. This amounts to an absorbing boundary condition at $r = a$. We refer to the region between the boundary at $r = d$ and the outer boundary at $r = a$ as the intermediate (mid) region (M).

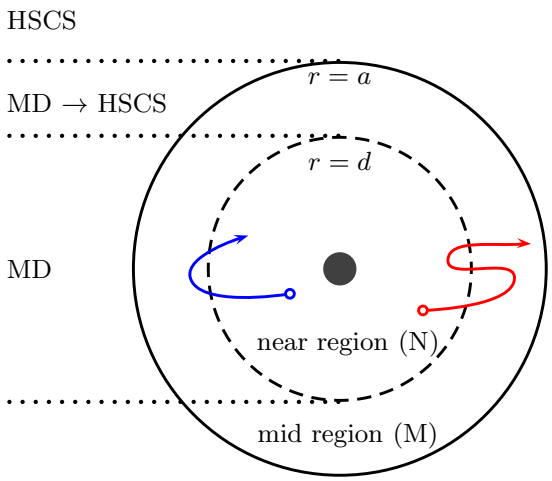

Figure S7: Partitioning of the space around the polarizing agent (dark circle) into near ($r < d$) and mid ($d < r < a$) regions, where the boundary $r = a$ is absorbing.[S14] In our analysis $a = 3.4$ nm for acetone in water and $a = 3.5$ nm for chloroform.

The correlation function $C^{\mathrm{NM}}(t)$ obeying the absorbing boundary condition can be accurately determined from MD simulations that are finite in spatial extent (Fig. S6b). On the other hand, the corresponding dipolar SDF $J^{\mathrm{NM}}(\omega)$ can be obtained analytically within the classical HSCS model but subjected to to an absorbing boundary condition at $r = a$ (denoted as HSCSa).[S14] The resulting analytical expression is parametrized by a diffusion constant D, and a "distance of closest approach" b. Fits to the MD-estimated $J^{\mathrm{NM}}(\omega)$ by the

HSCSa model are shown in the inset of Fig. S8. The best-fitting parameters are given in the NF column of Table S3. The desired SDFs $J^{\mathrm{NF}}(\omega)$, which correspond to an infinite region F, are obtained by letting $a \to \infty$ in the analytical expressions of the fitted $J^{\mathrm{NM}}(\omega)$. Thus, in a sense, we use the analytical expression of the HSCSa model to "unfold" the finite-extent $J^{\mathrm{NM}}(\omega)$ to an infinite-extent $J^{\mathrm{NF}}(\omega)$.

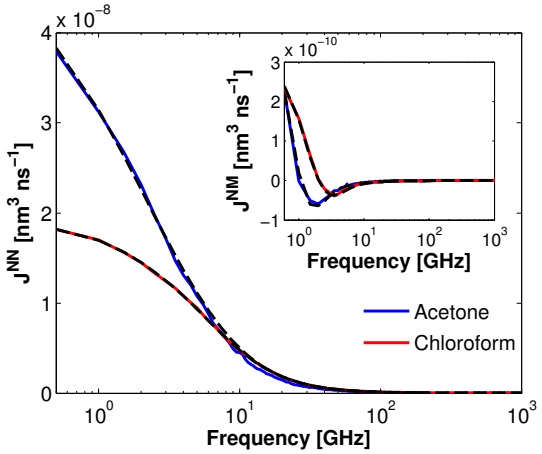

Figure S8: NN (main figure) and NM (inset) dipolar SDFs are in color. Their fits with the b and D parameters given in Table S3 are shown with black dashed lines.

Table S3: The fit parameters b (nm) and D (nm^2/ns) for acetone and chloroform.

		NN	NF	FF
Acetone	b	0.44	0.46	0.50
	D	1.35	1.70	1.53
Chloroform	b	0.46	0.50	0.52
	D	3.00	3.45	5.48

The same "unfolding" to infinite space should be applied even to the MD-estimated $J^{\mathrm{NN}}(\omega)$ since, in principle, molecular trajectories that contribute to $C^{\mathrm{NN}}(t)$ can cross into the F region and come back (Fig. S5, blue path). However, because the analytical HSCSa model assumes that the spins are at the centers of the (spherical) molecules, to perform this "unfolding" we calculate auxiliary $C^{\mathrm{NN}}(t)$ from the MD trajectories by pretending that the spins are at the centers of mass of the solvent and TEMPOL molecules (Fig. S6, dashed red lines). Clearly, the actual spin locations on the molecules become immaterial once the spins

are at a sufficiently large separation (Fig. S6b). MD-estimated $J^{\mathrm{NN}}(\omega)$ calculated from the center-of-mass (COM) positions can be fit directly with the analytical expression from the HSCSa model. These fits are shown in Fig. S8 and the best-fitting parameters are given in the NN column of Table S3.

After appropriately "unfolding" the MD-based $J^{\mathrm{NN}}(\omega)$ and $J^{\mathrm{NF}}(\omega)$, and calculating $J^{\mathrm{FF}}(\omega)$ using the HSCS model, the final dipolar SDF is obtained by adding all these contributions:

$$J(\omega) = J^{\mathrm{NN}}(\omega) + 2J^{\mathrm{NF}}(\omega) + J^{\mathrm{FF}}(\omega). \tag{11}$$

The functions $J(\omega)$ obtained for the two types of carbons of acetone and the carbon of chloroform are plotted with solid black lines in Fig. 3 of the main text.

Scalar SDF

Unlike the dipolar interaction, the scalar interaction is short-ranged. Therefore, for the scalar interaction, any reasonably-sized MD simulation box should automatically be "sufficiently large" such that applying the two-region unfolding procedure described above becomes unnecessary. Thus, it should be possible to base the estimate of the scalar TCF on the MD trajectories as such without any finite-size correction.

The Fermi contact depends on the electron spin density at the positions of the nuclei of interest. While the nuclear positions can be obtained from the MD snapshots, the determination of the electron spin density requires genuinely quantum mechanical calculations. For the treatment of the scalar interaction, therefore, we introduced a quantum region in which the free radical and a few solvent molecules around it are modeled in greater (quantal) detail than available from the (classical) MD simulations (Fig. S9).[S19] Differently from the near and mid regions introduced previously for the analysis of the dipolar interaction, the quantum region was not defined by a fixed distance from the center of mass of the free radical. Instead, a fixed number of solvent molecules whose centers of mass were closest to

the nitroxide oxygen atom, as well as the free radical itself, were included in the quantum region.[S19] With the so-defined quantum region, the scalar interaction between a given nucleus and the electron spin is either taken from the quantum mechanical (DFT) calculation if the nucleus is in the quantum region, or is automatically assigned as zero if the nucleus is outside the quantum region.

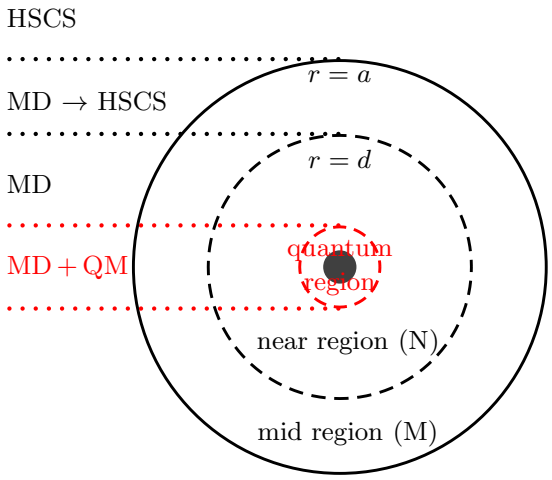

Figure S9: A schematic depiction of the quantum region (red) containing only a few solvent molecules closest to the oxygen atom of the nitroxide free radical. The scalar interaction is computed with *ab initio* calculations of the molecules in the quantum region as extracted from the MD snapshots. Thus, scalar SDF is obtained by combining the MD simulations with quantum mechanical calculations (MD + QM). The other two regions are necessary for the calculation of the dipolar SDF.

The time series of the Fermi contacts along the molecular trajectories, obtained either from DFT calculations or assigned as zero, are used to calculate the scalar TCFs as

$$C_{\text{iso}}(t) = \frac{(2\pi)^2}{N_I} \langle A_{\text{iso}}(\tau) A_{\text{iso}}(\tau + t) \rangle_\tau . \tag{12}$$

Here, $A_{\text{iso}}(t)$ denotes the Fermi contact at time t in units of MHz, the prefactor (2π) converts the units from Hz to rad/sec, the angular brackets denote averaging over the ensemble of molecules and over the time τ, and N_I is the number density of the nuclear spins. The resulting TCF is fitted to a sum of decaying exponential functions, as in the dipolar case.

The TCFs for the three studied ^{13}C nuclei and their multiexponential fits are shown in Fig. S10. The corresponding fitting parameters are given in Table S4.

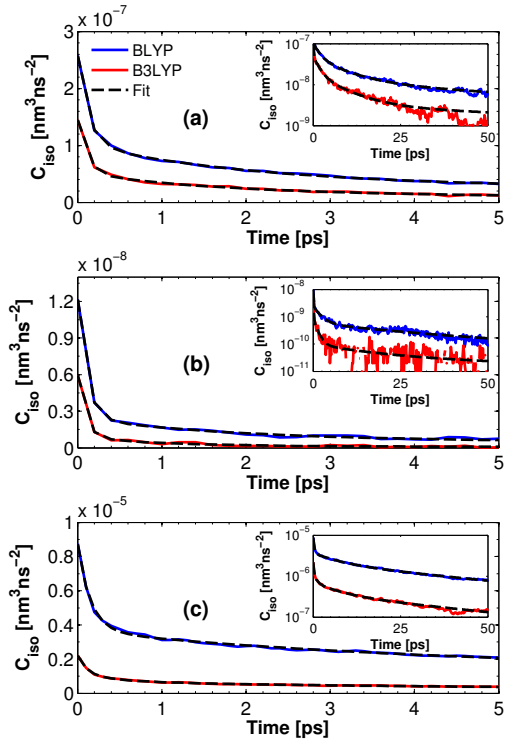

Figure S10: Scalar TCFs for (a) C_{H_3} and (b) C_O of acetone, and (c) carbon of chloroform are shown with colored solid lines and their exponential fits with dashed black lines. The same TCFs are shown for longer times in the insets. Fermi contacts calculated with the density functional B3LYP lead to the TCFs shown in red. The functional BYLP consistently leads to larger inter-molecular Fermi contacts, which produce the TCFs shown in blue.

The scalar TCFs obtained from DFT calculations with BLYP (blue lines) and B3LYP (red lines) are considerably different. As manifested by the exponential fit parameters, not only are the timescales of decay obtained from BLYP somewhat larger than those from B3LYP, but the magnitudes of the TCFs produced by BLYP are almost twice as large compared to those obtained using B3LYP.

When we compare the TCFs of different nuclei, C of chloroform is about 30 times larger than C_{H_3} of acetone, and 3 orders of magnitude larger than C_O of acetone. The scalar SDFs

Table S4: Multi-exponential fit parameters a_i (nm^{-3}) and τ_i (ps) for the scalar interaction for carbons of acetone (C_{H_3} and C_O) and chloroform (C).

C_{H_3}	B3LYP	a_i	0.093	0.034	0.015	0.003
		τ_i	0.110	1.599	7.918	131.2
	BLYP	a_i	0.154	0.059	0.033	0.011
		τ_i	0.123	1.768	8.525	88.94
C_O	B3LYP	a_i	0.005	0.001		
		τ_i	0.090	1.070		
	BLYP	a_i	0.010	0.002		
		τ_i	0.105	1.884		
C	B3LYP	a_i	1.045	0.454	0.348	0.359
		τ_i	0.107	0.450	3.422	25.07
	BLYP	a_i	5.039	1.626	2.038	0.020
		τ_i	0.151	3.421	25.31	76.15

are obtained from the scalar TCFs via one-sided Fourier transform:

$$K(\omega) = \int_0^\infty C_{\mathrm{iso}}(t) \mathrm{e}^{-\mathrm{i}\omega t} \mathrm{d}t. \tag{13}$$

Consequently, the scalar SDF of the carbon of chloroform is much larger than the scalar SDFs of the carbons of acetone (as shown in Fig. 3 of the main text).

Statistical uncertainty of the calculated coupling factors

In order to examine the statistical uncertainty of our estimated coupling factors due to the finite number of MD snapshots analyzed with DFT, the 10000 consecutive Fermi contact series were divided into two equal parts and analyzed separately. In the case of acetone, where coordinates were saved every 0.2 ps, each fragment of 5000 consecutive snapshots amounted to a duration of 1 ns. For chloroform, each fragment of 5000 consecutive snapshots amounted to a total duration of 0.5 ns because coordinates were saved every 0.1 ps.

The coupling factors of acetone calculated separately from the two fragments (1 and 2) are given in Table S5, which also contains the coupling factors calculated from the entire 10000 snapshots (1&2). The differences are tiny for the carbonyl carbon of acetone (C_O).

However, this is due to the negligibly small contribution of the scalar interaction. The contribution of the scalar coupling to the DNP of the methyl carbon of acetone is larger, thus we see larger differences between the coupling factors calculated from 5000 snapshots only.

The standard deviations (Δ) of the two independent 1 ns values are also included in the table. Note that the values of Δ obtained from the coupling factors determined independently from the two fragments, overestimate the actual uncertainties of the coupling factors that are obtained from the snapshots in both fragments by about a factor of $\sqrt{2}$.

The coupling factors calculated from two 0.5 ns fragments, and total 1 ns fragment of the chloroform trajectory are given in Table S6. The standard deviation between the two fragments is largest at 0.35 T and drops at the higher frequencies.

Table S5: DNP coupling factors (%) at 25 °C calculated for 5 M acetone in water. Dipolar SDF is obtained from the analysis of the entire 10 ns MD trajectory. Scalar SDF is obtained from the specified trajectory fragments. Fermi contacts were computed using the BLYP functional.

	fragment	0.35 T	1.2 T	3.4 T	9.2 T	16.4 T
C_O	1 (1 ns)	15.4	2.98	0.69	0.14	0.03
	2 (1 ns)	15.2	2.84	0.63	0.12	0.01
	1&2 (2 ns)	15.3	2.91	0.66	0.13	0.02
	Δ	0.1	0.07	0.03	0.01	0.01
C_{H_3}	1 (1 ns)	5.15	−2.27	−1.88	−0.95	−0.77
	2 (1 ns)	3.34	−3.30	−2.39	−1.21	−1.01
	1&2 (2 ns)	3.90	−2.67	−2.18	−1.07	−0.90
	Δ	1.3	0.73	0.36	0.18	0.17

Table S6: DNP coupling factors (%) at 25 °C for TEMPOL in chloroform. Dipolar SDF is obtained from the analysis of the entire 10 ns MD trajectory. Scalar SDF is obtained from the specified trajectory fragments. BLYP functional is used in all DFT calculations.

fragment	0.35 T	1.2 T	3.4 T	9.2 T	16.4 T
1 (0.5 ns)	−74.1	−63.1	−42.7	−27.0	−22.6
2 (0.5 ns)	−80.7	−64.5	−43.7	−26.0	−21.2
1&2 (1 ns)	−78.2	−64.3	−42.8	−26.3	−22.1
Δ	4.7	0.99	0.71	0.71	0.99

Validation of the point-dipole approximation

In addition to Fermi contacts (i.e., isotropic scalar couplings) DFT calculations also provide anisotropic hyperfine (i.e., dipolar) couplings. This allows us to investigate the accuracy of the point dipole approximation. When calculating dipolar TCFs from the atomic coordinates in the MD trajectories, we treat the electron spin as localized at the oxygen (50%) and nitrogen (50%) atoms of TEMPOL. However, the DFT calculations clearly show that the spin density is delocalized in space (see insets of Figs. 1c and 4b in the main text). Such delocalization is the reason for large Fermi contacts. As a result, the point-dipole approximation of the electron spin is expected to fail to describe the dipolar interaction with nearby nuclear spins.

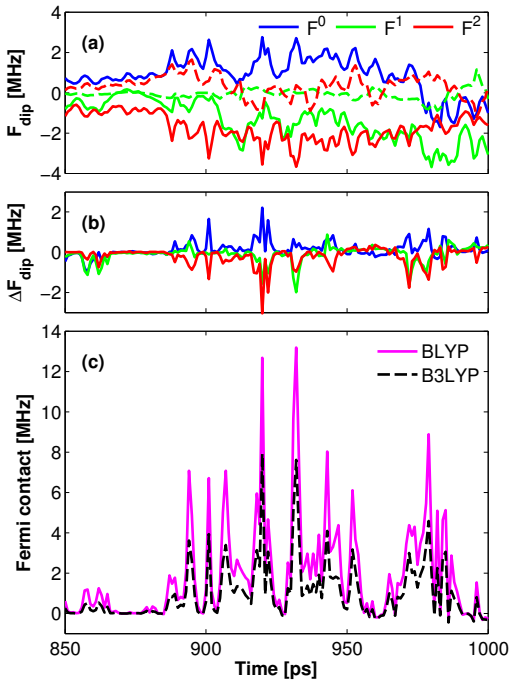

Figure S11: The dipolar and scalar couplings to a carbon of chloroform. In (a), the dipolar constants are calculated using the point-dipole approximation. Their difference from the coupling constant taken directly from the DFT calculations (i.e., without the point-dipole approximation) are given in (b). The Fermi contacts of the same atom are given in (c). Using the functional BLYP in the DFT calculations leads to systematically larger Fermi contacts compared to B3LYP.

Figure S11c shows the temporal variation of the Fermi contacts with the ^{13}C nucleus

on one chloroform molecule obtained from the DFT calculations over a time interval of 150 ps. (The same Fermi contacts are shown in Fig. 4 of the main text.) The solid harmonics describing the dipolar interaction between the electron spin and the nuclear spin of the same carbon atom over the same time period are given in Fig. S11a. These, however, were calculated from the distance vector between the atomic positions using (7). In other words, they reflect the dipolar interaction according to the point-dipole approximation. The same solid harmonics, but reflecting the dipolar coupling without assuming the point-dipole approximation, can be extracted from the anisotropic hyperfine couplings reported in the output files of the DFT calculations. (These are given in Fig. 4a of the main text.) The differences between the DFT and point-dipole values of F^m_{dip} are plotted in Fig. S11b. As expected, the point-dipole approximation fails at the instances exhibiting substantial Fermi contacts. On the other hand, the performance of the approximation is seen to be acceptable for the instances of small Fermi contacts. This implies that it can be safely used for molecules outside the quantum region, where the scalar couplings are vanishingly small anyway.

Although we have demonstrated the limitations of the point-dipole approximation, what matters from a practical point of view is the impact of the approximate treatment on the calculated DNP coupling factors. In order to assess the error in the predicted coupling factors caused by using the point-dipole approximation, we calculated dipolar TCFs from the 1-ns fraction of the MD simulation of TEMPOL in chloroform for which DFT calculations were carried out. The TCFs shown in red in Fig. S12 were calculated from the distance vector using the point-dipole approximation. In contrast, when calculating the TCFs shown in blue, the dipolar coupling constants were taken directly from the DFT calculations when the molecule was in the quantum region, and calculated using the point-dipole approximation when the molecule was outside the quantum region. A small difference is observed between the near-near (NN) TCFs, while the near-intermediate (NM) TCFs are practically identical.

DNP coupling factors were calculated using either one or the other of the two TCFs in Fig. S12 in order to assess the error due to the point-dipole approximation. Note that, in

this case, only 1 ns of the MD trajectory is used to calculate both the dipolar and the scalar spectral densities. The resulting coupling factors are given in Table S7. The differences between the coupling factors are seen to be small and less than the statistical uncertainties estimated in Table S6. Thus, although the methodology we have developed allows us to go beyond the point-dipole approximation when calculating the dipolar SDF, we find that the statistical uncertainty due to estimating the scalar SDF from only 10000 MD snapshots is larger.

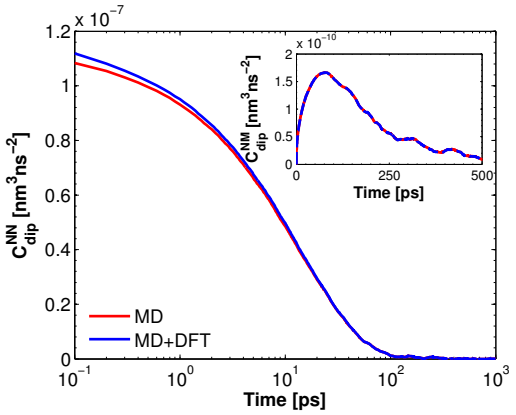

Figure S12: Near-near and near-intermediate (inset) dipolar TCFs of chloroform obtained from a 1 ns fragment of the MD trajectories. The contributions of molecules in the quantum region are calculated by using the point-dipole approximation (red) and DFT calculations (blue).

Table S7: DNP coupling factors (%) of chloroform calculated from 1 ns fraction of the MD simulations. Dipolar contributions for the molecules in the quantum region are calculated by either point-dipole approximation or DFT calculations. BLYP functional is used in all DFT calculations.

Field (Tesla)	0.35	1.2	3.4	9.2	16.4
point dipole	−78.2	−64.8	−43.4	−26.9	−22.6
DFT + p.d.	−77.8	−64.4	−43.1	−26.6	−22.4
Δ	0.3	0.3	0.2	0.2	0.14

We can also compare the coupling factors produced from dipolar analysis of 1 ns MD trajectory (Table S7) and the entire 10 ns trajectory (Table S6). For all examined magnetic fields the difference is less than 1%, suggesting good convergence of the dipolar SDF in 1

ns. Therefore, we conclude that the estimate of $J(\omega)$ from the full 10 ns simulation must be rather precise.

References

(S1) Phillips, J. C.; Braun, R.; Wang, W.; Gumbart, J.; Tajkorshid, E.; Villa, E.; Chipot, C.; Skeel, R. D.; Kale, L.; Schulten, K. *J. Comp. Chem.* **2005**, *26*, 1781–1802.

(S2) Vanommeslaeghe, K.; Hatcher, E.; Acharya, C.; Kundu, S.; Zhong, S.; Shim, J.; Darian, E.; Guvench, O.; Lopes, P.; Vorobyov, I.; Mackerell, A. D. *J. Comput. Chem.* **2010**, *31*, 671–690.

(S3) Sezer, D.; Freed, J. H.; Roux, B. *J. Phys. Chem. B* **2008**, *112*, 5755–5767.

(S4) Lingwood, M. D.; Han, S. *J. Magn. Reson.* **2009**, *201*, 137 – 145.

(S5) Küçük, S. E.; Neugebauer, P.; Prisner, T. F.; Sezer, D. *Phys. Chem. Chem. Phys.* **2015**, *17*, 6618–6628.

(S6) McDonald, N. A.; Carlson, H. A.; Jorgensen, W. L. *Journal of Physical Organic Chemistry* **1997**, *10*, 563–576.

(S7) Yaws, C. L. *Thermodynamic and Physical Property Data*; Gulf Publishing, 1992.

(S8) Chandra, R.; Xu, M.; Firman, P.; Eyring, E. M.; Petrucci, S. *J. Phys. Chem.* **1993**, *97*, 12127–12133.

(S9) Frisch, M. J.; Trucks, G. W.; Schlegel, H. B.; Scuseria, G. E.; Robb, M. A.; Cheeseman, J. R.; Scalmani, G.; Barone, V.; Mennucci, B.; Petersson, G. A.; Nakatsuji, H.; Caricato, M.; Li, X.; Hratchian, H. P.; Izmaylov, A. F.; Bloino, J.; Zheng, G.; Sonnenberg, J. L.; Hada, M.; Ehara, M.; Toyota, K.; Fukuda, R.; Hasegawa, J.; Ishida, M.;

Nakajima, T.; Honda, Y.; Kitao, O.; Nakai, H.; Vreven, T.; Montgomery, J. A., Jr.; Peralta, J. E.; Ogliaro, F.; Bearpark, M.; Heyd, J. J.; Brothers, E.; Kudin, K. N.; Staroverov, V. N.; Kobayashi, R.; Normand, J.; Raghavachari, K.; Rendell, A.; Burant, J. C.; Iyengar, S. S.; Tomasi, J.; Cossi, M.; Rega, N.; Millam, J. M.; Klene, M.; Knox, J. E.; Cross, J. B.; Bakken, V.; Adamo, C.; Jaramillo, J.; Gomperts, R.; Stratmann, R. E.; Yazyev, O.; Austin, A. J.; Cammi, R.; Pomelli, C.; Ochterski, J. W.; Martin, R. L.; Morokuma, K.; Zakrzewski, V. G.; Voth, G. A.; Salvador, P.; Dannenberg, J. J.; Dapprich, S.; Daniels, A. D.; Farkas, Ö.; Foresman, J. B.; Ortiz, J. V.; Cioslowski, J.; Fox, D. J. Gaussian09 Revision D.01. Gaussian Inc. Wallingford CT 2009.

(S10) Tomasi, J.; Mennucci, B.; Cammi, R. *Chem. Rev.* **2005**, *105*, 2999–3094.

(S11) Barone, V. In *Recent advances in density functional methods, part I.*; Chong, D., Ed.; World Scientific Publ. Co., Singapore, 1997.

(S12) Schäfer, A.; Huber, C.; Ahlrichs, R. *J. Chem. Phys.* **1994**, *100*, 5829–5835.

(S13) Marenich, A. V.; Cramer, C. J.; Truhlar, D. G. *J. Phys. Chem. B* **2009**, *113*, 6378–6396.

(S14) Sezer, D. *Phys. Chem. Chem. Phys.* **2013**, *15*, 526–540.

(S15) Sezer, D. *Phys. Chem. Chem. Phys.* **2014**, *16*, 1022–1032.

(S16) Ayant, Y.; Belorizky, E.; Alizon, J.; Gallice, J. *J. Phys. (Paris)* **1975**, *36*, 991–1004.

(S17) Hwang, L.-P.; Freed, J. H. *J. Chem. Phys.* **1975**, *63*, 4017–4025.

(S18) Fries, P. H.; Imbert, D.; Melchior, A. *J. Chem. Phys.* **2010**, *132*, 044502–11.

(S19) Küçük, S. E.; Biktagirov, T.; Sezer, D. *Phys. Chem. Chem. Phys.* **2015**, *17*, 24874–24884.